OCEANOGRAPHY

Highly variable upper and abyssal overturning cells in the South Atlantic

M. Kersalé[1,2]*, C. S. Meinen[2], R. C. Perez[2], M. Le Hénaff[1,2], D. Valla[3], T. Lamont[4,5], O. T. Sato[6], S. Dong[2], T. Terre[7], M. van Caspel[6], M. P. Chidichimo[3,8,9], M. van den Berg[4], S. Speich[10], A. R. Piola[3,9,11], E. J. D. Campos[6,12], I. Ansorge[5], D. L. Volkov[1,2], R. Lumpkin[2], S. L. Garzoli[1,2]

The Meridional Overturning Circulation (MOC) is a primary mechanism driving oceanic heat redistribution on Earth, thereby affecting Earth's climate and weather. However, the full-depth structure and variability of the MOC are still poorly understood, particularly in the South Atlantic. This study presents unique multiyear records of the oceanic volume transport of both the upper (<~3100 meters) and abyssal (>~3100 meters) overturning cells based on daily moored measurements in the South Atlantic at 34.5°S. The vertical structure of the time-mean flows is consistent with the limited historical observations. Both the upper and abyssal cells exhibit a high degree of variability relative to the temporal means at time scales, ranging from a few days to a few weeks. Observed variations in the abyssal flow appear to be largely independent of the flow in the overlying upper cell. No meaningful trends are detected in either cell.

INTRODUCTION

The fundamental role played by the Meridional Overturning Circulation (MOC) in redistributing mass, heat, salt, and carbon within the global climate system is well recognized (*1*, *2*). The intensity of the MOC is related to the rate of deep ocean ventilation and thereby connects the time scales of heat uptake and carbon storage (*1*). Despite its importance, direct observations of the MOC in the Atlantic before the past decade or two were fairly limited in spatial and temporal coverage, particularly in the South Atlantic (*3*). As a result, present scientific knowledge is largely based on model simulations. Numerical models have suggested that Atlantic MOC variations and stability can originate and/or be controlled via interbasin exchanges of heat and especially salt across the South Atlantic gateway connecting the Atlantic with the other ocean basins (*4*, *5*). The traditional view is that there are two complete MOC cells in the South Atlantic Ocean, with an upper cell that involves northward transports above ~1000 m and a lower ("abyssal") cell that involves Antarctic Bottom Water (AABW) northward transports below ~4000 to 4500 m (Fig. 1) (*6*–*9*). These northward transports are compensated by southward-flowing North Atlantic Deep Water (NADW) between those two northward-flowing layers, which completes the upper and abyssal overturning cells as depicted in Fig. 1. The complexities of these two interconnected cells make the South Atlantic unique; it is the only ocean basin with an equatorward net heat transport (*10*, *11*) that modulates interhemispheric global atmospheric circulations on decadal time scales (*12*).

Given the importance of understanding South Atlantic MOC (SAMOC) variations, substantial resources have been invested in observing these flows over the past two decades. However, most of the MOC volume, heat, and/or salt transport estimates in the South Atlantic have been based on infrequent trans-basin observations from ships, including quasi-decadal full-depth conductivity-temperature-depth

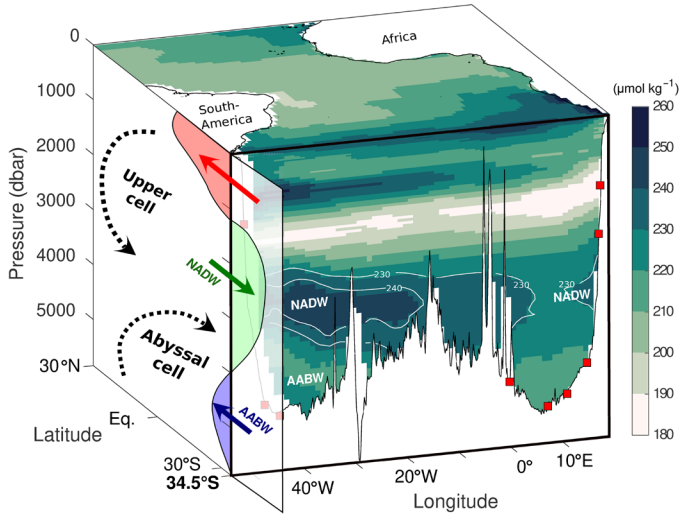

Fig. 1. Array locations and simple schematic of water mass overturning transports. Study area with shaded colors representing oxygen concentrations (μmol kg^{-1}) at the surface and along the 34.5°S SAMBA line from the World Ocean Atlas 2018 annual climatology (*38*). The tongues of elevated oxygen concentrations along the western and eastern boundaries identify different branches of recently ventilated NADW as it crosses 34.5°S (white contours). Locations of the nine SAMBA moorings used for computing the zonally integrated meridional geostrophic flow are represented as red squares. Conceptual schematics of the volume transport across 34.5°S and of the upper and abyssal Atlantic overturning cells are indicated on the left side of the panel. Colors indicate the classes of seawater density (red, shallow and intermediate; green, deep; blue, abyssal).

[1]Cooperative Institute for Marine and Atmospheric Studies, University of Miami, Miami, FL, USA. [2]NOAA Atlantic Oceanographic and Meteorological Laboratory, Miami, FL, USA. [3]Servicio de Hidrografía Naval, Buenos Aires, Argentina. [4]Oceans and Coasts Research Branch, Department of Environmental Affairs, Cape Town, South Africa. [5]Department of Oceanography, University of Cape Town, Rondebosch 7701, South Africa. [6]Oceanographic Institute, University of São Paulo, São Paulo, Brazil. [7]IFREMER, University of Brest, CNRS, IRD, Laboratoire d'Océanographie Physique et Spatiale (LOPS), IUEM, Plouzané, France. [8]Consejo Nacional de Investigaciones Científicas y Técnicas (CONICET), Argentina. [9]Instituto Franco-Argentino sobre Estudio del Clima y sus Impactos (UMI-IFAECI/CNRS-CONICET-UBA), Buenos Aires, Argentina. [10]Laboratoire de Météorologie Dynamique–IPSL, Ecole Normale Supérieure, Paris, France. [11]Universidad de Buenos Aires, Buenos Aires, Argentina. [12]Department of Biology, Chemistry and Environmental Sciences, School of Arts and Sciences, American University of Sharjah, Sharjah, United Arab Emirates.
*Corresponding author. Email: marion.kersale@noaa.gov

sections (*13*–*15*) and quasi-quarterly expendable bathythermograph (XBT) transects (*11*, *16*, *17*). Indirect estimates have also been made using blends of data from satellites (altimetry) and Argo profiling floats irregularly distributed in space and time (*18*, *19*). These studies have improved our understanding of the MOC across multiple latitudes in the South Atlantic. However, continuous multiyear daily records of the MOC upper cell in the North Atlantic (*20*) and preliminary analyses of daily moored data in the South Atlantic (*21*, *22*) have shown that infrequent snapshot measurements inevitably alias energetic high-frequency signals into seasonal and longer time scales. Furthermore, many of these infrequent and/or indirect observations provide measurements of only the upper water column, failing to capture important interannual-to-decadal deep density variations across the Atlantic Basin (*23*, *24*). This study addresses these shortcomings by producing the first-ever continuous daily time series capturing the full-depth MOC volume transports along 34.5°S.

We estimated the daily full-depth MOC volume transport using in situ observations of ocean bottom pressure and acoustic round-trip travel times from nine pressure-equipped inverted echo sounder (PIES) moorings in the SAMOC Basin-wide Array (SAMBA) at 34.5°S (Fig. 1). Geographically, this latitude serves as a gateway that connects the Atlantic Basin with flows from the Indian, Pacific, and Southern Oceans. Preliminary SAMBA efforts to estimate the strength of the MOC volume transport focused solely on the upper cell and used only the two shallowest PIES moorings (1350-dbar isobath) on either side of the basin (*21*, *22*). Here, we horizontally and vertically extend this analysis to resolve the daily transport from the surface down to ~4700 dbar during a 4-year period (September 2013 to July 2017) using data from nine moorings across 34.5°S (see the Supplementary Materials for additional data details).

RESULTS

The resulting time-mean structure of the MOC flows is illustrated by the time-mean profile of cumulative transport as a function of depth (Fig. 2A). The MOC upper cell (red line in Fig. 2A) is found above 3155 dbar (black dot), while the MOC abyssal cell (blue line) is found below this interface. The strength of the upper cell is calculated as the basin-wide transport integrated from the surface down to the time-mean pressure interface where the zonally integrated meridional flow changes from northward to southward (1315 dbar; red dot). The strength of the abyssal cell is calculated by integrating from the zero crossing of the cumulative transport as a function of depth (3155 dbar; black dot) down to the interface where the flow changes from southward to northward (4295 dbar; blue dot). The resulting volume transport variabilities are not sensitive to modest O(500 m) changes in these fixed interface levels, nor by allowing time variability in these levels (see the Supplementary Materials).

The time-mean meridional volume transport from September 2013 to July 2017 is 17.3 ± 5.0 sverdrup (Sv) northward in the upper cell (time mean ± bias; 1 Sv = 10^6 m^3 s^{-1}; see the Supplementary Materials) and 7.8 ± 2.7 Sv southward in the abyssal cell. The Atlantic and Arctic Basins are essentially closed in the extreme north, aside from the roughly 1 Sv of flow through the Bering Strait, which is nearly canceled by the evaporation minus precipitation integrated over the entire Atlantic Basin (*6*). Given that, mass conservation requires that the transport integrated over the full depth of the

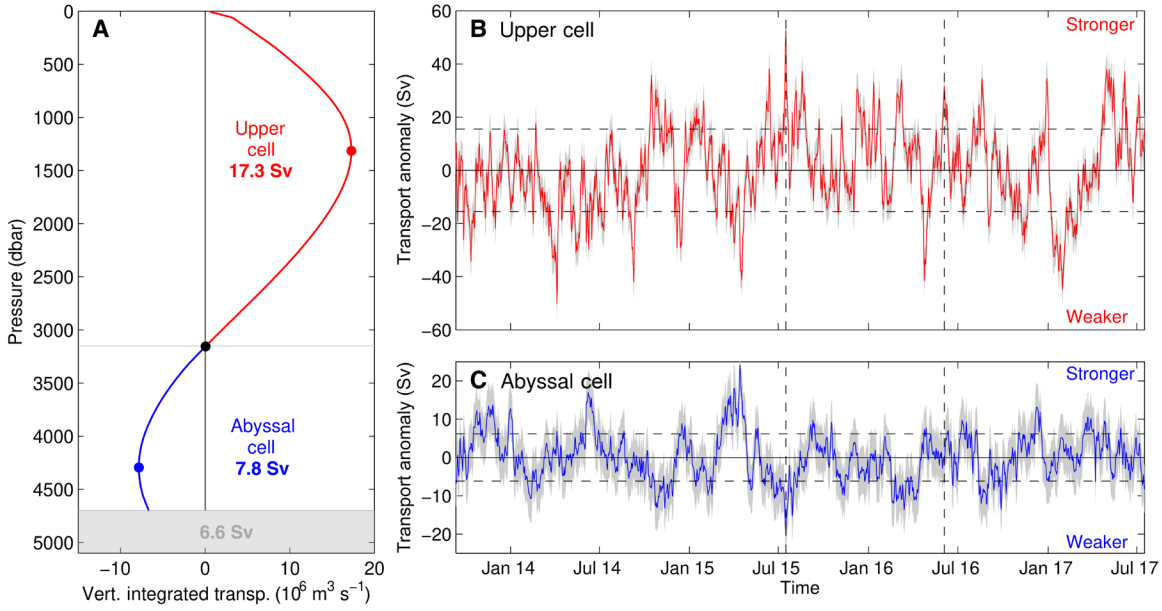

Fig. 2. Volume transports within the upper and abyssal cells: Mean structure and temporal variability. (**A**) Estimate of the September 2013 to July 2017 time-mean basin-wide vertically integrated (or cumulative) volume transport as a function of depth at 34.5°S with the upper cell highlighted in red and the abyssal cell in blue. The gray layer at the bottom of the panel represents the layer of unobserved flow below the deepest common depth of the interior moorings. The red and blue dots highlight the time-mean pressure interfaces where the zonally integrated meridional flow changes from northward to southward within the upper and abyssal cells, respectively. The black dot indicates the transition between the upper and abyssal cells. (**B**) Temporal anomalies of the upper cell transport (defined positive northward). (**C**) Temporal anomalies of the abyssal cell transport (defined positive southward). (B and C) Gray shading indicates the estimated daily accuracy as derived in the Supplementary Materials. Vertical dashed lines (B and C) illustrate events affecting both cells (July 2015) or only one of the cells (June 2016). Horizontal dashed lines (B and C) indicate anomalies exceeding the time-mean value by ±1 standard deviation; positive anomalies correspond to stronger cell transports, and negative anomalies indicate weaker transports. Sv, sverdrup.

ocean across SAMBA must be close to zero. SAMBA allows transport calculations from the surface down to 4700 dbar, yielding a time-mean southward transport of 6.6 ± 2.7 Sv integrated between the surface and this depth (Fig. 2A). This mean flow should equal the northward flow that crosses 34.5°S below 4700 dbar to close the mass budget. Historical estimates that have used inverse models and trans-basin hydrographic sections near this latitude have suggested a mean northward flow of about 2.4 ± 1.2 Sv below 4700 dbar (*6*). Given the error bar estimates, and the difference in time period between the historical observations and these new results, the net flow integrated from the surface to the bottom closes fairly well.

The enhanced resolution afforded by using nine moorings across 34.5°S shows a somewhat stronger and deeper time-mean upper cell than the previous estimate derived from the two shallowest moorings [14.7 Sv (*22*)], but the differences are within the range of error estimates for the calculations. The time-mean strength of the upper cell is also close to the available mean estimates near 34.5°S from quasi-quarterly XBT transects [17.9 to 18.1 Sv (*16*, *17*)], snapshot trans-basin hydrographic cruises [11.7 to 21.5 Sv (*15*)], and Argo- and satellite-derived MOC products [19.5 to 20.7 Sv (*18*, *19*)]. Historical estimates of the abyssal cell strength in this region are far fewer in number, coming solely from snapshot basin-wide hydrographic sections between latitudes ranging from 24°S to 32°S [5.5 Sv (*13*), 1.8 to 5.5 Sv (*6*), 3.5 to 7.0 Sv (*14*), 3.9 Sv (*7*), and 3.0 to 10.4 Sv (*15*)]. Numerical modeling studies have generally found weaker abyssal cell estimates than previous observational estimates (*9*). Perhaps, the most robust historical estimates of the strength of the AABW flow come from moored measurements in the channels to the north. The seafloor topography in the region dictates that most of the AABW that successfully flows northward from the Argentine Basin to the Brazil Basin (beyond ~32°S) must pass through the Vema or the Hunter Channels (*25*, *26*). Historical observations show a total northward AABW transport of ~4 Sv (*25*) and ~3 Sv (*26*) through the Vema and Hunter Channels, respectively. To the east of the Mid-Atlantic Ridge, the Cape Basin is essentially topographically closed to the north by the Walvis Ridge, thus preventing any contribution of AABW in that region to the large-scale overturning circulation (*27*). The ~7 Sv of northward-flowing AABW observed historically in Vema and Hunter Channels matches remarkably well with our independent estimate here of 7.8 ± 2.7 Sv for the southward upper limb of the abyssal cell.

DISCUSSION

Both the upper and abyssal cells exhibit strong variations at time scales, ranging from a few days to a few weeks (Fig. 2, B and C), highlighting the necessity for a continuous-in-time trans-basin observing system. The upper cell exhibits a daily temporal standard deviation of 15.5 Sv, about 2.5 times larger than the abyssal cell standard deviation of 6.2 Sv. The upper cell transport standard deviation greatly exceeds the variability found in prior model analyses in the region (*28*). Preliminary estimates calculated with the Estimating the Circulation and Climate of the Ocean, phase 2 (ECCO2) model (described in Materials and Methods) also show weaker variability in both cells and a weaker ratio of 1.5 between the upper and abyssal transport variability. The ECCO2 model does not assimilate SAMBA observations, so this represents a fully independent comparison. The difference in observed transport variability between the upper and abyssal cells is more than can be accounted for simply because the ocean grows narrower longitudinally with increasing depth. The integration area for the upper layer is roughly a factor of 1.5 larger than for the deeper layer, while as noted earlier, the upper layer variability is closer to a factor of 2.5 larger than that of the deep layer. A key result evident in both of these time series is the high degree of variability they exhibit relative to the temporal means. These large anomaly events last from 1 to 50 days and can occur simultaneously in both cells, e.g., the July 2015 barotropic event when the upper cell strengthened and the abyssal cell weakened (vertical dashed lines in Fig. 2, B and C). They can also occur in only one of the cells, e.g., June 2016 (vertical dashed lines in Fig. 2, B and C). The correlation coefficient between the upper and abyssal cell time series (without flipping the sign of the abyssal transport) is $r = 0.4$, which is significantly different from zero at the 95% confidence level based on the estimated 45 degrees of freedom (*29*). Some indication of statistically significant coherence (*30*) between the records is found on monthly and submonthly time scales; however, the coherences are still low at those periods, and overall, the coherence spectra are noisy. Despite the significant coherence and correlation, their low values indicate that transport variability in the abyssal cell is largely independent of the variations in the upper cell during this 4-year time period.

The daily MOC standard deviation at 34.5°S in the upper cell (15.5 Sv; reducing to 14.6 or 13.0 Sv with a 10- or 30-day low-pass filter applied, respectively) exceeds the previous estimate of 8.3 Sv from the pilot array (*21*, *22*), likely due to better capturing of the barotropic variations and eddies [e.g., Agulhas Rings (*17*)] using the full array resolution. The monthly 13.0-Sv standard deviation also exceeds those calculated from quarterly XBT transects [2.3 Sv (*17*)] and the products derived from satellite and Argo profile data [3.5 Sv (*18*)], as should be expected given the reduced temporal resolution of these observations. The variability derived from this study also exceeds that observed in the North Atlantic (2.7 Sv with a 10-day filter at 26°N and 3.3 Sv from monthly averages using the Overturning in the Subpolar North Atlantic Program), consistent with previous analyses suggesting that the MOC variability decreases northward (*23*, *31*, *32*). There are positive trends in the transports of both cells (stronger upper cell and weaker abyssal cell), but these trends are not statistically different from zero.

Spectral analysis of the transport time series of both cells confirms that the MOC is more energetic in the upper cell than in the abyssal cell at all time scales from periods of a few days to a year (compare Fig. 3, A and B). At subseasonal time scales, the spectra exhibit common peaks of energy in both cells (e.g., at 50 days), while at other period bands, high energy is observed only in the upper cell (12 to 20 days; gray shaded area in Fig. 3A). Levels of high energy are observed between intraseasonal and annual periods in both the upper and abyssal cells; however, note that the accuracy of the spectra at those time scales is limited due to the relatively short length of the analyzed record. Spectral distributions may yield more nuanced results once a few more years of data have been collected. Estimates of the associated seasonal cycle in the transport of both cells (Fig. 3, C and D) show that the upper cell (Fig. 3C) is consistent with the pilot study (*22*), with semi-annual periods of maximum transport in July to August and December to January. The seasonal cycle of the abyssal cell (Fig. 3D) is also semi-annual; however, it is roughly 180° out of phase with the cycle of the upper cell from March to October but closer to being in phase for the rest of the year. This likely reflects topographically imposed differences in the internal waves transmitting the seasonal forcing information (*33*).

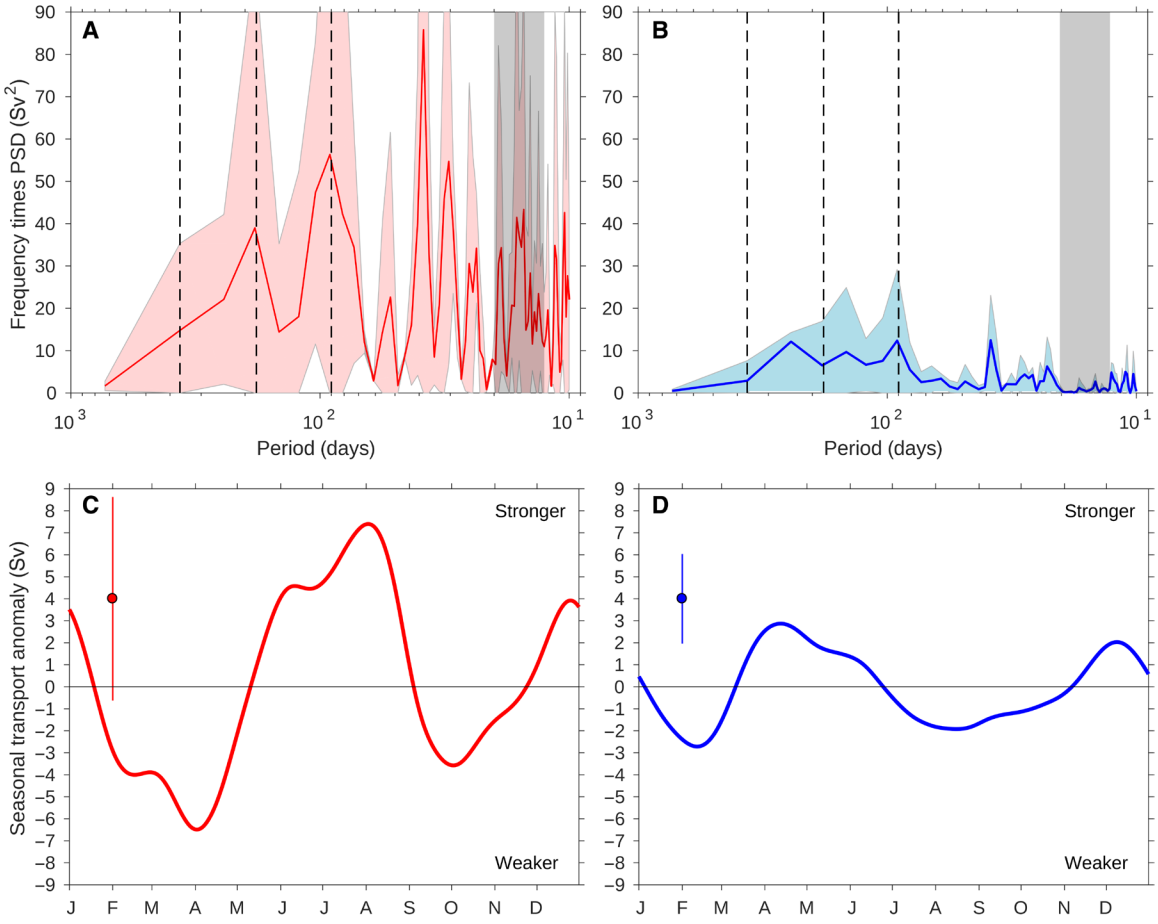

Fig. 3. Energy distributions and seasonal anomalies of the MOC volume transports. Variance-preserving spectra of the upper cell (**A**, red) and abyssal cell (**B**, blue) volume transports. Spectra were determined using Welch's averaged periodogram method and a 2-year window allowing 1 year of overlap. Red and blue shading areas indicate the 95% confidence limits based on the methods in (*29*), with colors matching the corresponding time series. Vertical black dashed lines indicate the annual, semi-annual, and 3-month periods (from left to right). Shaded gray area illustrates the 12- to 20-day period band, with high energy in the upper cell and low energy in the abyssal cell. Seasonal cycle of the upper cell (**C**, positive northward) and abyssal cell (D, positive southward) volume transport time series. Error bars indicated in the upper left represent ±1 standard error (see the Supplementary Materials for details), with colors matching the corresponding time series.

These 4 years of data from the SAMBA array have provided remarkable insights on the full-depth structure and variability of the MOC. Longer time series will be necessary, however, to confirm the details of seasonal to interannual variability and to detect possible long-term trends.

MATERIALS AND METHODS

We define the strength of the upper cell as the transport of the northward-flowing upper layer, which must be balanced in steady state by an equal transport of a southward-flowing NADW layer. Likewise, we define the strength of the abyssal cell as the southward transport of the deeper NADW layers, which must be balanced by northward-flowing AABW transport in a steady state. The approach with the SAMBA instruments is to infer full water-column profiles of dynamic height from vertical acoustic travel times via the Gravest Empirical Mode method (*34*). These estimates are combined with directly measured ocean bottom pressure values to compute both the geostrophic relative ("baroclinic") and geostrophic reference ("barotropic") components of the meridional flows, respectively, between each pair of moored instruments. The barotropic flow is directly determined from the ocean bottom pressure measurements. Our method of obtaining the barotropic flow is in contrast to the zero-net-flow constraint commonly applied as part of MOC computations at some of the North Atlantic arrays (*31*, *32*, *35*, *36*). However, bottom pressure sensors can only quantify the temporal variability of the barotropic velocity, not the time mean. The time-mean reference velocity at 1500 dbar is therefore included from a 26-year run of the ECCO2 ocean state estimate (https://ecco.jpl.nasa.gov/). The 1992–2018 time mean from the ECCO2 model output, with horizontal resolution along the SAMBA latitude of 1/4°, is also used to provide a time-mean estimate of the meridional flows inshore of the shallowest moorings on either side of the basin ("boundary"). The daily wind-driven meridional Ekman flow is derived from the Cross-Calibrated Multi-Platform (CCMP) zonal wind stress (*37*) for the same time period as the moored data. The baroclinic, barotropic, boundary, and Ekman terms are combined and zonally integrated across the basin along 34.5°S to compute the total daily meridional transport per unit depth (details and an error analysis are presented in the Supplementary Materials).

SUPPLEMENTARY MATERIALS

Supplementary material for this article is available at http://advances.sciencemag.org/cgi/content/full/6/32/eaba7573/DC1

REFERENCES AND NOTES

1. IPCC, *Climate Change 2013: The Physical Science Basis*, T. F. Stocker, D. Qin, G.-K. Plattner, M. B. Tignor, S. K. Allen, J. Boschung, A. Nauels, Y. Xia, V. Bex, P. M. Midgley, Eds. (Cambridge Univ. Press, 2013).
2. S. Rahmstorf, G. Feulner, M. E. Mann, A. Robinson, S. Rutherford, E. J. Schaffernicht, Exceptional twentieth-century slowdown in Atlantic Ocean overturning circulation. *Nat. Clim. Change* **5**, 475–480 (2015).
3. M. Rhein, Taking a close look at ocean circulation. *Science* **363**, 456–457 (2019).
4. A. Biastoch, C. W. Böning, J. R. E. Lutjeharms, Agulhas leakage dynamics affects decadal variability in Atlantic overturning circulation. *Nature* **456**, 489–492 (2008).
5. W. Weijer, W. Cheng, S. S. Drijfhout, A. V. Federov, A. Hu, L. C. Jackson, W. Liu, E. L. McDonagh, J. V. Mecking, J. Zhang, Stability of the atlantic meridional overturning circulation: A review and synthesis. *J. Geophys. Res.* **124**, 5336–5375 (2019).
6. R. Lumpkin, K. Speer, Global ocean meridional overturning. *J. Phys. Oceanogr.* **37**, 2550–2562 (2007).
7. L. D. Talley, Closure of the global overturning circulation through the Indian, Pacific, and Southern Oceans: Schematics and transports. *Oceanography* **26**, 80–97 (2013).
8. D. Valla, A. R. Piola, C. S. Meinen, E. Campos, Strong mixing and recirculation in the northwestern Argentine Basin. *J. Geophys. Res.* **123**, 4624–4648 (2018).
9. P. Cessi, The global overturning circulation. *Ann. Rev. Mar. Sci.* **11**, 249–270 (2019).
10. A. Ganachaud, C. Wunsch, Improved estimates of global ocean circulation, heat transport and mixing from hydrographic data. *Nature* **408**, 453–457 (2000).
11. S. L. Garzoli, M. O. Baringer, Meridional heat transport determined with expandable bathythermographs—Part II: South Atlantic transport. *Deep Sea Res. Part I* **54**, 1402–1420 (2007).
12. H. Lopez, S. Dong, S. K. Lee, G. Goni, Decadal modulations of interhemispheric global atmospheric circulations and monsoons by the South Atlantic meridional overturning circulation. *J. Climate* **29**, 1831–1851 (2016).
13. E. L. McDonagh, B. A. King, Oceanic fluxes in the South Atlantic. *J. Phys. Oceanogr.* **35**, 109–122 (2005).
14. H. L. Bryden, B. A. King, G. D. McCarthy, South Atlantic overturning circulation at 24°S. *J. Mar. Res.* **69**, 39–56 (2011).
15. A. Hernández-Guerra, L. D. Talley, J. L. Pelegrí, P. Vélez-Belchí, M. O. Baringer, A. M. Macdonald, E. L. McDonagh, The upper, deep, abyssal and overturning circulation in the Atlantic Ocean at 30°S in 2003 and 2011. *Prog. Oceanogr.* **176**, 102136 (2019).
16. S. Dong, S. L. Garzoli, M. O. Baringer, C. S. Meinen, G. J. Goni, Interannual variations in the Atlantic meridional overturning circulation and its relationship with the net northward heat transport in the South Atlantic. *Geophys. Res. Lett.* **36**, L20606 (2009).
17. S. L. Garzoli, M. O. Baringer, S. Dong, R. C. Perez, Q. Yao, South Atlantic meridional fluxes. *Deep-Sea Res. I Oceanogr. Res. Pap.* **71**, 21–32 (2013).
18. S. Dong, G. J. Goni, F. Bringas, Temporal variability of the South Atlantic meridional overturning circulation between 20°S and 35°S. *Geophys. Res. Lett.* **42**, 7655–7662 (2015).
19. S. Majumder, C. Schmid, G. Halliwell, An observations and model-based analysis of meridional transports in the South Atlantic. *J. Geophys. Res.* **121**, 5622–5638 (2016).
20. T. Kanzow, S. A. Cunningham, W. E. Johns, J. J.-M. Hirschi, J. Marotzke, M. O. Baringer, C. S. Meinen, M. P. Chidichimo, C. Atkinson, L. M. Beal, H. L. Bryden, J. Collins, Seasonal variability of the Atlantic meridional overturning circulation at 26.5°N. *J. Climate* **23**, 5678–5698 (2010).
21. C. S. Meinen, S. Speich, R. C. Perez, S. Dong, A. R. Piola, S. L. Garzoli, M. O. Baringer, S. Gladyshev, E. J. D. Campos, Temporal variability of the meridional overturning circulation at 34.5°S: Results from two pilot boundary arrays in the South Atlantic. *J. Geophys. Res.* **118**, 6461–6478 (2013).
22. C. S. Meinen, S. Speich, A. R. Piola, I. J. Ansorge, E. J. D. Campos, M. Kersalé, T. Terre, M. P. Chidichimo, T. Lamont, O. T. Sato, R. C. Perez, D. Valla, M. A. van den Berg, M. Le Hénaff, S. Dong, S. L. Garzoli, Meridional Overturning Circulation transport variability at 34.5°S during 2009-2017: Baroclinic and barotropic flows and the dueling influence of the boundaries. *Geophys. Res. Lett.* **45**, 4180–4188 (2018).
23. E. Frajka-Williams, M. Lankhorst, J. Koelling, U. Send, Coherent circulation changes in the Deep North Atlantic from 16°N and 26°N transport arrays. *J. Geophys. Res.* **123**, 3427–3443 (2018).
24. D. Desbruyères, E. L. McDonagh, B. A. King, V. Thierry, Global and full-depth ocean temperature trends during the early twenty-first century from argo and repeat hydrography. *J. Climate* **30**, 1985–1997 (2017).
25. N. Hogg, P. E. Biscaye, W. D. Gardner, W. J. Schmitz Jr., On the transport and modification of Antarctic Bottom Water in the vema channel. *J. Mar. Res.* **40**, 231–263 (1982).
26. W. Zenk, G. Siedler, B. Lenz, N. G. Hogg, Antarctic bottom water flow through the hunter channel. *J. Phys. Oceanogr.* **29**, 2785–2801 (1999).
27. M. Arhan, H. Mercier, Y. H. Park, On the deep water circulation of the eastern South Atlantic Ocean. *Deep-Sea Res. I Oceanogr. Res. Pap.* **50**, 889–916 (2003).
28. R. C. Perez, S. L. Garzoli, C. S. Meinen, R. P. Matano, Geostrophic velocity measurement techniques for the meridional overturning circulation and meridional heat transport in the South Atlantic. *J. Atmos. Oceanic Tech.* **28**, 1504–1521 (2011).
29. R. E. Thomson, W. J. Emery, *Data Analysis Methods in Physical Oceanography* (Elsevier Science, ed. 3, 2014), pp. 728.
30. R. O. R. Y. Thompson, Coherence significance levels. *J. Atmos. Sci.* **36**, 2020–2021 (1979).
31. S. A. Cunningham, T. Kanzow, D. Rayner, M. O. Baringer, W. E. Johns, J. Marotzke, H. R. Longworth, E. M. Grant, J. J.-M. Hirschi, L. M. Beal, C. S. Meinen, H. L. Bryden, Temporal variability of the Atlantic meridional overturning circulation at 26.5°N. *Science* **317**, 935–938 (2007).
32. T. Kanzow, S. A. Cunningham, D. Rayner, J. J.-M. Hirschi, W. E. Johns, M. O. Baringer, H. L. Bryden, L. M. Beal, C. S. Meinen, J. Marotzke, Observed flow compensation associated with the MOC at 26.5°N in the Atlantic. *Science* **317**, 938–941 (2007).
33. O. A. Saenko, On the strong seasonal currents in the deep ocean. *J. Climate* **21**, 5642–5656 (2008).
34. C. S. Meinen, D. R. Watts, Vertical structure and transport on a transect across the North Atlantic current near 42°N: Time series and mean. *J. Geophys. Res.* **105**, 21869–21891 (2000).
35. G. D. McCarthy, D. A. Smeed, W. E. Johns, E. Frajka-Williams, B. I. Moat, D. Rayner, M. O. Baringer, C. S. Meinen, J. Collins, H. L. Bryden, Measuring the Atlantic meridional overturning circulation at 26°N. *Prog. Oceanogr.* **130**, 91–111 (2015).
36. M. S. Lozier, F. Li, S. Bacon, F. Bahr, A. S. Bower, S. A. Cunningham, M. F. de Jong, L. de Steur, B. deYoung, J. Fischer, S. F. Gary, B. J. W. Greenan, N. P. Holliday, A. Houk, L. Houpert, M. E. Inall, W. E. Johns, H. L. Johnson, C. Johnson, J. Karstensen, G. Koman, I. A. Le Bras, X. Lin, N. Mackay, D. P. Marshall, H. Mercier, M. Oltmanns, R. S. Pickart, A. L. Ramsey, D. Rayner, F. Straneo, V. Thierry, D. J. Torres, R. G. Williams, C. Wilson, J. Yang, I. Yashayaev, J. Zhao, A sea change in our view of overturning in the subpolar North Atlantic. *Science* **363**, 516–521 (2019).
37. R. Atlas, R. N. Hoffman, J. Ardizzone, S. M. Leidner, J. C. Jusem, D. K. Smith, D. Gombos, A cross-calibrated, multiplatform ocean surface wind velocity product for meteorological and oceanographic applications. *Bull. Amer. Meteor. Soc.* **92**, 157–174 (2011).
38. H. E. Garcia, K. Weathers, C. R. Paver, I. Smolyar, T. P. Boyer, R. A. Locarnini, M. M. Zweng, A. V. Mishonov, O. K. Baranova, D. Seidov, J. R. Reagan, World Ocean Atlas 2018, Volume 3: *Dissolved Oxygen, Apparent Oxygen Utilization, and Oxygen Saturation*, A. Mishonov Technical Ed. (NOAA Atlas NESDIS 83, 2018).
39. M. Kersalé, R. C. Perez, S. Speich, C. S. Meinen, T. Lamont, M. Le Hénaff, M. A. van den Berg, S. Majumder, I. J. Ansorge, S. Dong, C. Schmid, T. Terre, S. L. Garzoli, Shallow and deep eastern boundary currents in the South Atlantic at 34.5°S: Mean structure and variability. *J. Geophys. Res.* **124**, 1634–1659 (2019).
40. K. A. Donohue, D. R. Watts, K. L. Tracey, A. D. Greene, M. Kennelly, Mapping circulation in the Kuroshio extension with an array of current and pressure recording inverted echo sounders. *J. Atmos. Ocean. Tech.* **27**, 507–527 (2010).

Acknowledgments: We would like to express our great appreciation to the captains, officers, and crews of the research vessels who have supported our work. We are also very grateful to the support and technical staff who have helped collect and process the data presented herein, particularly R. F. Garcia who processed all of the PIES data. We also thank S.-K. Lee, G. Derr, and the two anonymous reviewers for helpful comments. **Funding:** The U.S. PIES observations and the participation of C.S.M., R.C.P., and S.D. were supported via the NOAA Climate Program Office-Ocean Observing and Monitoring Division (FundRef no. 100007298) under the Southwest Atlantic Meridional Overturning Circulation ("SAM") project. M.L.H. and M.K. acknowledge additional support from NASA (grant 80NSSC18K0773). D.L.V., M.K., M.L.H., and S.L.G. were supported in part under the auspices of the Cooperative Institute for Marine and Atmospheric Studies (CIMAS), a Cooperative Institute of the University of Miami and NOAA (cooperative agreement NA10OAR4320143), and/or under a grant from the NOAA Climate Variability Program (GC16-212). C.S.M., D.L.V., M.K., M.L.H., R.L., R.C.P., S.D., and S.L.G. also acknowledge additional support from the NOAA Atlantic Oceanographic and Meteorological Laboratory. S.S. and T.T. acknowledge support from the 11-ANR-56-004 SAMOC research project. S.S. also received support from the European Union Horizon 2020 research and innovation program under grant agreement 633211 (AtlantOS). E.J.D.C., M.v.C. and O.T.S. acknowledge the São Paulo State Research Foundation (FAPESP, grants 2011/50552-4, 2017/09659-6, 2018/09823-3, and 2019/07833-4), the Brazilian Navy (DHN and SeCIRM), and the University of São Paulo (Oceanographic Institute) for support through the SAMOC-Br project. E.J.D.C. also acknowledges CNPq for a Research Fellowship (grant 302018/2014-0). I.A., M.v.d.B., and T.L. acknowledge support from the DST-NRF-SANAP programme and the South African DEA. The Argentine cruises were supported by Servicio de Hidrografía Naval and

CONICET. Additional support for A.R.P., D.V., E.J.D.C., and M.P.C. was provided by the Inter-American Institute for Global Change Research grant CRN3070 (U.S. NSF grant GEO-1128040). **Author contributions:** A.R.P., S.S., E.J.D.C., C.S.M., I.A., S.L.G., R.C.P., S.D., and M.L.H. conceptualized and initiated the SAMBA project and/or related projects and acquired financial support leading to this publication. All authors were involved in data collection and methodology development. M.K., C.S.M., R.C.P., M.L.H., D.V., S.S., and R.L. conducted the research and/or aided in the analysis. M.K. led the writing of the manuscript with additional content and/or editorial contributions from all the co-authors. **Competing interests:** The authors declare that they have no competing interests. **Data and materials availability:** All data needed to evaluate the conclusions in the paper are present in the paper and/or the Supplementary Materials. Additional data related to this paper may be requested from the authors. The CCMP version 2.0 wind product was created by Remote Sensing Systems and is made available on the web at www.remss.com. ECCO2 output is available at https://ecco.jpl.nasa.gov/. The data used herein from the South Atlantic MOC Basin-wide Array (SAMBA) can be found at www.aoml.noaa.gov/phod/SAMOC_international/index.php.

Submitted 2 January 2020
Accepted 25 June 2020
Published 5 August 2020
10.1126/sciadv.aba7573

Citation: M. Kersalé, C. S. Meinen, R. C. Perez, M. Le Hénaff, D. Valla, T. Lamont, O. T. Sato, S. Dong, T. Terre, M. van Caspel, M. P. Chidichimo, M. van den Berg, S. Speich, A. R. Piola, E. J. D. Campos, I. Ansorge, D. L. Volkov, R. Lumpkin, S. L. Garzoli, Highly variable upper and abyssal overturning cells in the South Atlantic. *Sci. Adv.* **6**, eaba7573 (2020).